Title

TRANSMISSION ELECTRON MICROSCOPY CHARACTERIZATION OF DISLOCATED ""LATH"" MARTENSITE

Author

Rao, B.V.N.

Publication Date

1979-04-01

To be presented at the International
Conference on Martensitic Transformations,
Boston, MA, June 24-29, 1979

TRANSMISSION ELECTRON MICROSCOPY CHARACTERIZATION OF DISLOCATED "LATH" MARTENSITE

B. V. Narasimha Rao and G. Thomas

April 1979

Prepared for the U. S. Department of Energy
under Contract W-7405-ENG-48

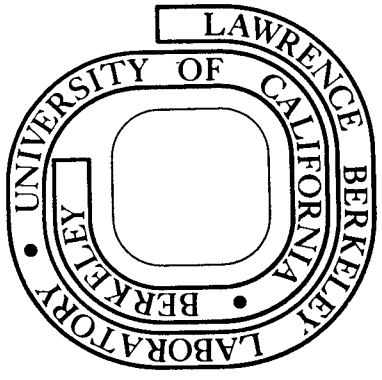

DISCLAIMER

TRANSMISSION ELECTRON MICROSCOPY CHARACTERIZATION OF DISLOCATED "LATH" MARTENSITE

B. V. Narasimha Rao and G. Thomas *
University of California

Department of
Materials Science and Mineral Engineering
and
Materials and Molecular Research Division
Lawrence Berkeley Laboratory
Berkeley, California 94720

ABSTRACT

In this paper, a summary of the recent observations made with high resolution transmission electron microscopy on the morphology, crystallography and formation of "lath" martensite is presented. The present work has confirmed earlier observations that within each packet the adjacent "laths" are separated by rotation boundaries, such that a 180° rotation of the reference shear vector is achieved in a group of adjacent laths. The number of laths required to achieve this rotation decreases as the carbon content is increased from 0 to 0.4 wt.%. Concomitant with this, the tendency for adjacent twin related laths increases with carbon content. Retained austenite is found only in carbon containing alloys and even in these alloys it is found only if the adjacent laths are not twin related. High resolution lattice imaging at the retained austenite/lath martensite interface has revealed substantial carbon segregation in austenite during the shear transformation and this raises fundamental questions in regard to whether "lath" martensites are truly martensitic. Lattice imaging also revealed the presence of interfacial ledges at the retained austenite/lath martensite interface.

Introduction

There are two basic morphologies of bulk martensite in ferrous alloys (1-3): dislocated lath martensite and twinned plate martensite. The former is usually associated with steels for carbon contents of less than about 0.4 wt.% with a total alloy content such that the M_s is not far

---

Invited speaker: International Conference on Martensitic Transformations, June 24-29, 1979, Boston, Mass.

below about 250°C. Plate martensites occurring in steels of high alloy concentrations have been extensively studied (1,4) and the crystallography of this transformation is well understood (1,5). However, as has been pointed out previously (6) a complete understanding of the crystallography, the transformation mechanism and the precise morphology of the technologically more important lath martensite is lacking. As a result of detecting austenite in these steels (7,8) however, it has been shown (6) that direct crystallographic analysis on austenite serves to eliminate scatter in the published crystallographic data (9,10) for the lath martensite transformation.

Several important questions remain unanswered regarding the mechanism of the lath martensite formation. For example, the independent nucleation and growth events of this transformation are not clearly established (11-14). Studies using two adjacent lath orientations yielded no concrete results on the accommodation of shape strain for this transformation (15,16). In particular, the above aspects have to be re-examined in the light of the identification of retained austenite. This paper is a summary of a detailed characterization of lath martensite using conventional, high resolution and high voltage transmission electron microscopy to be reported in full elsewhere (17) and is a continuation of the work first reported at the Kiev Conference in 1977 (6).

Experimental Procedures

Compositions of the alloys used in this investigation are listed in Table I. The iron-nickel alloys available in the form of thin sheets were first encapsulated in evacuated quartz tubes and austenitized for 1 hour followed by quenching into iced water. The quartz capsule was broken immediately after its contact with the quenching medium. The medium carbon (0.3 wt.%) steels were austenitized in bulk at 1100°C for 1 hour followed by quenching into iced water or oil. However, for alloy 5 and for the 0.4%C alloy interrupted quenching in the M_s-M_f range was necessary in order to avoid intergranular quench cracking (18). Some of the medium carbon steels were also subjected to grain refining double treatments. Details about these heat-treatments and specimen preparation are discussed elsewhere (18,19). Thin foils made by jet polishing were examined in a Philips EM301 microscope at 100 KV and also in a Hitachi HU650 high voltage

microscope at 500 KV. The latter was used to utilize the higher resolution capabilities for selected area diffraction (SAD) associated with higher voltages due to lower spherical aberration effects. Detailed SAD analyses were performed on arrays of packets in the alloys studied (Table I). Lattice imaging was done in the Philips EM301 microscope using tilted beam illumination (20). Laser optical microdiffraction was subsequently conducted to analyze the lattice fringe images (21).

Results

(i) Morphology and Substructure of Martensite

Figures 1 and 2 show examples of a group of dislocated laths within a packet of the binary Fe-5%Ni and the Fe/3Cr/0.5Mo/2Mn/0.3C alloys respectively. The laths in all the alloys are characterized by fairly straight boundaries except for the curvature at the packet boundaries. The average lath width of the carbon containing alloys is smaller than that of the carbon free alloys (cf. Figs. 1 and 2). Interlath retained austenite has been identified only in the carbon containing alloys, Fig. 3, but not in Fe/Mo/C steels in agreement with previous studies (6, 22). In addition, in the 0.3C and 0.4C alloys, quite frequently interweaving packets belonging to two different variants of the habit plane and interference from nucleation of the laths belonging to other variants has been observed.

(ii) Orientation Analysis of a Group of Adjacent Laths in the Packets

Analysis of many alloys show that two main types of lath orientations occur. In carbon-less alloys, the martensite packets generally consist of groups of parallel laths each lath being separated by successive rotations about $\langle 110 \rangle_m$ or occasionally $\langle 100 \rangle_m$ until the n^{th} lath is 180^o rotated from the first (6). The value of n varies but on the average it is five or more (Fig. 1) for the binary Fe-Ni alloys. On the other hand, in the carbon containing alloys, the laths are often twin related. In this case, of course, n=2. Figure 4 shows twin related laths in a 0.3%C steel. The bright-field image contrast clearly shows the identical orientations of laths 1, 3, 5 etc. and of the alternate twin laths 2, 4 etc. This is also confirmed by the SAD patterns. On the average n=3 for the medium carbon steels, Fig. 2.

It is important to emphasize here that the interface twinning plane

for adjacent twin related laths in 0.3%C alloys is frequently $\{110\}_m$ and not the $\{112\}_m$. However, the latter has been observed occasionally in 0.3%C alloys and quite extensively in the 0.4%C steel (alloy 9). Associated with $\{112\}_m$ twin related laths is the change in habit plane for the transformation from the widely observed (6) $\{110\}_m$ to the $\{112\}_m$. Also, when the interface plane is $\{110\}_m$, then the two adjacent laths, twin related, have identical $\langle 111\rangle_m$ SAD patterns which superimpose as one pattern if the SAD records both. This point is an important one since this effect has been universally overlooked by other investigators.

(iii) Morphology, Occurrence and Crystallography of Retained Austenite

Figure 3 shows a typical example of the continuous, thin interlath films of retained austenite in the carbon containing alloys. The dark-field micrograph of this figure also reveals retained austenite at packet boundaries. Significantly, retained austenite is absent at those lath boundaries for which the adjacent lath orientations correspond to a twin relation, Fig. 4. This is true for both $\{110\}_m$ and $\{112\}_m$ twins.

Both Kurdjumov-Sachs (K-S) and Nishiyama-Wasserman (N-W) orientation relations are widely observed in the alloys used. In addition both K-S and N-W relations are found to be obeyed frequently within the same packet (10) (for example, the SAD pattern of Fig. 3 shows this). Also, a new result is found in a few instances viz., the Bain orientation relation between retained austenite and lath martensite. In this case, interestingly the lath rotation axis is observed to be $\langle 100\rangle_m$, e.g., Fig. 1.

Direct habit plane analysis on retained austenite confirmed the $\{111\}_a$ habit plane for this transformation (6).

(iv) Carbon Analysis

High resolution lattice imaging can be performed to estimate the carbon content of retained austenite since carbon is below the resolution limits of x-ray STEM techniques. Details of the method are discussed elsewhere (17). Figure 5 shows an example of the simultaneous lattice imaging of $\{101\}_m$ and $\{111\}_a$ planes (an extremely difficult experiment). From the fringe spacings, analyzed directly and by laser optical diffraction, the lattice parameters c and a were estimated from established formulae (23) as follows:

$$c(\text{Å}) = 2.8664 + 0.1162(x) \qquad (1)$$

$$a(\text{Å}) = 2.8664 - 0.01303(x) \qquad (2)$$

where x is weight % carbon. For calculating the room temperature lattice parameter of the austenite, the following equation is employed (23):

$$a_o(\mathring{A}) = 3.555 + 0.044(x) \qquad (3)$$

The data are given in Table II. these are for alloy 5 only, but are typical.

The above results indicate significant carbon enrichment in austenite varying between a minimum of 0.41 wt.% and a maximum of 1.04 wt.%.

(v) Structure of the Austenite-Martensite Interface

The lattice imaging (Fig. 5) experiments also provide detailed information about interfaces (20). In Fig. 5 there are three different fringes: (1) the {110} martensite fringes on either side of the austenite region, (2) the {111} austenite fringes and (3) the larger periodicity structural moiré fringes at the interface. Figure 5 shows that the retained austenite/lath martensite interface exhibits a high degree of coherence. Occasional terminating fringes in either phase have been observed indicating that some of the elastic strain is accommodated by interfacial dislocations. Interestingly, the lattice fringes in both phases are fairly straight right up to the interface but very close to the interface drastic bending takes place to maintain coherency. The structural moiré, Fig. 5, for the first time reveals the presence of interfacial ledges several unit cells high at the retained austenite/lath martensite interface. The presence of these ledges has already been proposed (6) to account for the scatter in the habit plane analysis. By changing the ledge density and morphology, a curved macroscopic lath boundary can be generated while maintaining a unique microscopic habit plane. This then accounts for the curved interfaces for the laths particularly close to their packet boundaries, for example in Fig. 4.

Discussion

The observations in this paper suggest that the following transformation paths are followed in the austenite-martensite lath situation:

1. Twin related laths grow cooperatively to minimize strain energy from a common interface plane -- the twinning plane in autensite {viz., $(111)_\gamma \rightarrow (110)_m$ or $(112)_m$}. No retained austenite should then ever occur between such laths (as is observed).
2. Non-twin related laths also nucleate successively and cooperatively. The principal shear direction is however rotated during successive nucleations. This explains the orientation relationships

(each lath rotated from its precursor until a full 180° has been achieved, Fig. 6). The retained austenite is then trapped between these laths; it is highly deformed -- also probably as a result of accommodation of the transformation strains. This austenite is so stabilized but as shown it is also chemically stabilized by carbon enrichment which will drive the M_s to very low temperatures. The resultant block of rotated laths is such that the net shear across the block is zero (analogous to the successive 1/6 $[11\bar{2}]$ + 1/6 $[1\bar{2}1]$ + 1/6 $[\bar{2}11]$ shears to minimize strain and shape deformation in the fcc - hcp transformation; in this case the rotation is successively 60°).

For the carbonless alloys, twin related laths are rarely seen and the adjacent lath orientations correspond to case 2 above without the inter-lath retained austenite.

The observation that both K-S and N-W relations are found to be alternating within the same martensite packet of most of the alloys investigated needs explanation. If the transformation is nucleation limited, then it can be greatly aided if there are a larger number of variants available for martensite nucleation. This is explained by the stereographic analysis shown in Figure 6. The number of orientations for nucleation increases from two for purely K-S to three for combined K-S and N-W, i.e., a 50% gain in nucleation flexibility (Path 1, Fig. 6). Path 2 indicates the alternate twin related nucleation path.

The observation of the Bain relation means that a different habit plane other than $\{110\}_m$ occurs and this is probably partly responsible for some scatter in the habit plane analysis by indirect methods. On the other hand, the Bain relation provides a different rotation axis for the laths in a packet, i.e., $\langle 100\rangle_m$ (Fig. 1) as opposed to the most frequently observed $\langle 110\rangle_m$, Figs. 2-4. This again provides for increased flexibility in the nucleation and shape accommodation.

Figure 4 shows a unique example of the degree of accommodation necessary at the impingement site of three packets in the medium carbon steels. First, the laths in the central packet are twin-related. Second, the rotation axes for the adjoining packets are rotated 70° and 110° with respect to $\langle 110\rangle_m$ rotation axes in the central packet. Further minimization of the volume dependent strain energy at the impingement sites can be discerned from the decrease in lath widths at the packet boundaries.

In addition, some $\{112\}_m$ substructural (probably accommodation) twinning is seen in the packet at the upper right hand side, Fig. 4.

An interesting example of the rotation of the shear vector and the resultant upheavals in the lateral direction at a packet boundary is provided by the bright-field (BF) and dark-field (DF) micrographs of Fig. 3.

Summary and Conclusions

(1) Retained austenite has been observed only in carbon containing alloys. Direct analysis on the austenite yielded a single $\{111\}_a$ habit plane, i.e., a $\{110\}_m$ plane including the twin interface plane in twin related laths. The only exception to this is the $\{112\}_m$ twin interface plane and when the Bain relationship is seen.

(ii) In order to minimize the strain energy, the shear components in a group of laths must add up to a 180° rotation. Since the strain energy increases with %C, this rotation is most simply obtained by twinning. In non-twin related laths (lower %C) successive laths are rotated in varying degrees with stabilized retained austenite between them which also plays a part in accommodation.

(iii) In the medium carbon alloys a high degree of accommodation of shape strain is also seen in the form of interweaving packets and reduced lath widths at the packet boundaries.

(iv) Lattice imaging revealed ledges at the retained austenite lath martensite interface confirming earlier predictions (6). In addition, lattice imaging indicates substantial carbon enrichment of austenite which is important in its stabilization. Except for the twin related laths, the presence of interlath retained austenite suggests that the individual laths are the fundamental nucleation and growth events.

(v) The present study confirms the morphology of lath martensite proposed earlier; they are indeed thin platelets with their thickness undergoing a slight reduction at the packet boundaries.

(vi) The question should then be asked -- in lath martensite containing interlath retained austenite, since carbon enrichment (and hence, diffusion) occurs, is the transformation really martensitic? The structure can be described as incomplete upper bainite (complete upper bainite contains interlath carbides, e.g., from a $\gamma \rightarrow Fe_3C$ type reaction at the lath interface).

Acknowledgements

This work was performed under the auspices of the U.S. Dept. of Energy under contract No. W7405-Eng-48 through the Materials and Molecular Research Division of the Lawrence Berkeley Laboratory. We thank Mr. M. Sarikaya for his help with this paper. The lattice imaging work (B.V.N.R.) has been supported by NSF (Grant #DMR 72-03269 A01).

References

(1) C. M. Wayman: Metallography, 8(1975), 105.
(2) G. Thomas: Iron and Steel Intl., 46(1973), 451.
(3) G. Krauss and A. R. Marder: Met. Trans., 2(1971), 2343.
(4) A. B. Grenninger and A. R. Troiano: Trans. AIME, 140(1940), 307.
(5) M. Umemoto and C. M. Wayman: Aeta Met., 26(1978). 1529.
(6) G. Thomas and B. V. N. Rao: Proc. International Conf. on Martensite, ICOMAT-77, Kiev, USSR, (1978), 57.
(7) B. V. Narasimha Rao, J. Y. Koo and G. Thomas: Proc. EMSA, Ed. by G. W. Bailey, Claitors Pub. Div., Baton Rouge, Louisiana, (1975), 30.
(8) G. Thomas: Met. Trans. A., 9A(1978), 439.
(9) D. S. Sarma, J. A. Whiteman, and J. H. Woodhead: Metal. Sci. J., 10(1976), 391.
(10) B. V. Narasimha Rao: Met. Trans. A., (1979), in press.
(11) M. J. Roberts: Met. Trans., 1(1970), 3287.
(12) J. S. Pascover and S. V. Radcliffe: Acta Met., 17(1969) 321.
(13) J. M. Oblak and R. F. Heheman: Transformation and Hardenability in Steels, Climax Moly Co., Ann Arbor, Michigan, (1967), 15.
(14) F. J. Schoen and W. S. Owen: Metallography, 3(1970), 473.
(15) J. M. Chilton, C. J. Barton and G. R. Speich: JISI, 208(1970), 184.
(16) G. R. Speich and P. R. Swann: JISI, 203(1965), 480.
(17) B. V. Narasimha Rao and G. Thomas: Met. Trans. A., to be published.
(18) B. V. Narasimha Rao and G. Thomas: Mat. Sci. and Engin., 20(1975), 195.
(19) B. V. Narasimha Rao and G. Thomas: Met. Trans. A., in press.
(20) J. G. Allpress and J. V. Sanders: J. Appl. Cryst., 6(1973), 165.
(21) R. Sinclair and G. Thomas: Met. Trans. A., 9A(1978), 373.
(22) R. B. G.Yeo: Trans. AIME, 224(1962), 1222.
(23) J. M. Moyer and G. S. Ansell: Met. Trans. A., 6A(1975), 1785.

Figure Captions

Fig. 1 - Detailed analysis of orientations of martensite laths in a packet of the binary Fe-15Ni alloy.

(a) Bright-field micrograph with laths identified by 1, 2, 3, etc.

(b) SAD patterns from laths identified by 1, 2, 3, etc. in (a).

(c) Stereographic analysis showing rotations of laths 1 through 5.

Fig. 2 - Detailed analyses of a group of martensite laths in a packet of Fe/3Cr/2Mn/0.5Mo/0.3C alloy:

(a) Bright-field micrograph and the corresponding SAD analysis and,

(b) Stereographic analysis of rotations of adjacent laths.

Fig. 3 - Bf (a), DF (b) and analyzed SAD pattern (c) showing retained austenite in Fe/3Cr/2Ni/0.5Mo/0.3C alloy.

Fig. 4 - BF and the corresponding SAD patterns revealing adjacent twin related laths in a packet martensite of Fe/3Cr/2Mn/0.5Mo/0.3C steel.

Fig. 5 - Lattice image micrograph of retained austenite/lath martensite interface in Fe/4Cr/5Ni/0.3C steel. $\{101\}_m$ fringes are imaged in martensite and $\{111\}_a$ fringes in austenite.

Fig. 6 - Stereographic illustration of successive lath rotations in a packet assuming both K-S and N-W relations are obeyed (Path 1). Path 2 corresponds to adjacent twin related laths.

Table I. Compositions of the Alloys and Their M_s Temperatures

Alloy #	Nominal Composition Wt.%	M_s, °C
1	Fe-12Ni	300*
2	Fe-15Ni	250*
3	Fe-20Ni	165*
4	Fe-4Cr-0.3C	320
5	Fe-4Cr-5Ni-0.3C	210
6	Fe-4Cr-2Mn-0.3C	253
7	Fe-3Cr-0.5Mo-2Mn-0.3C	320
8	Fe-3Cr-0.5Mo-2Ni-0.3C	330
9	Fe-4Cr-0.4C	320

* Calculated temperatures

Table II. Calculation of Retained Austenite Carbon Content (wt.%) in Fe/4Cr/5Ni/0.27C alloys from lattice images

Martensite d-spacing in 0.27 %C Steel at room temp.	Direct Measurement	Optical Diffractogram Measurement
d_{110_m} = 2.0244Å	0.55 wt.%	--
d_{011_m} = 2.0366Å	1.04 wt.%	0.41 wt.%

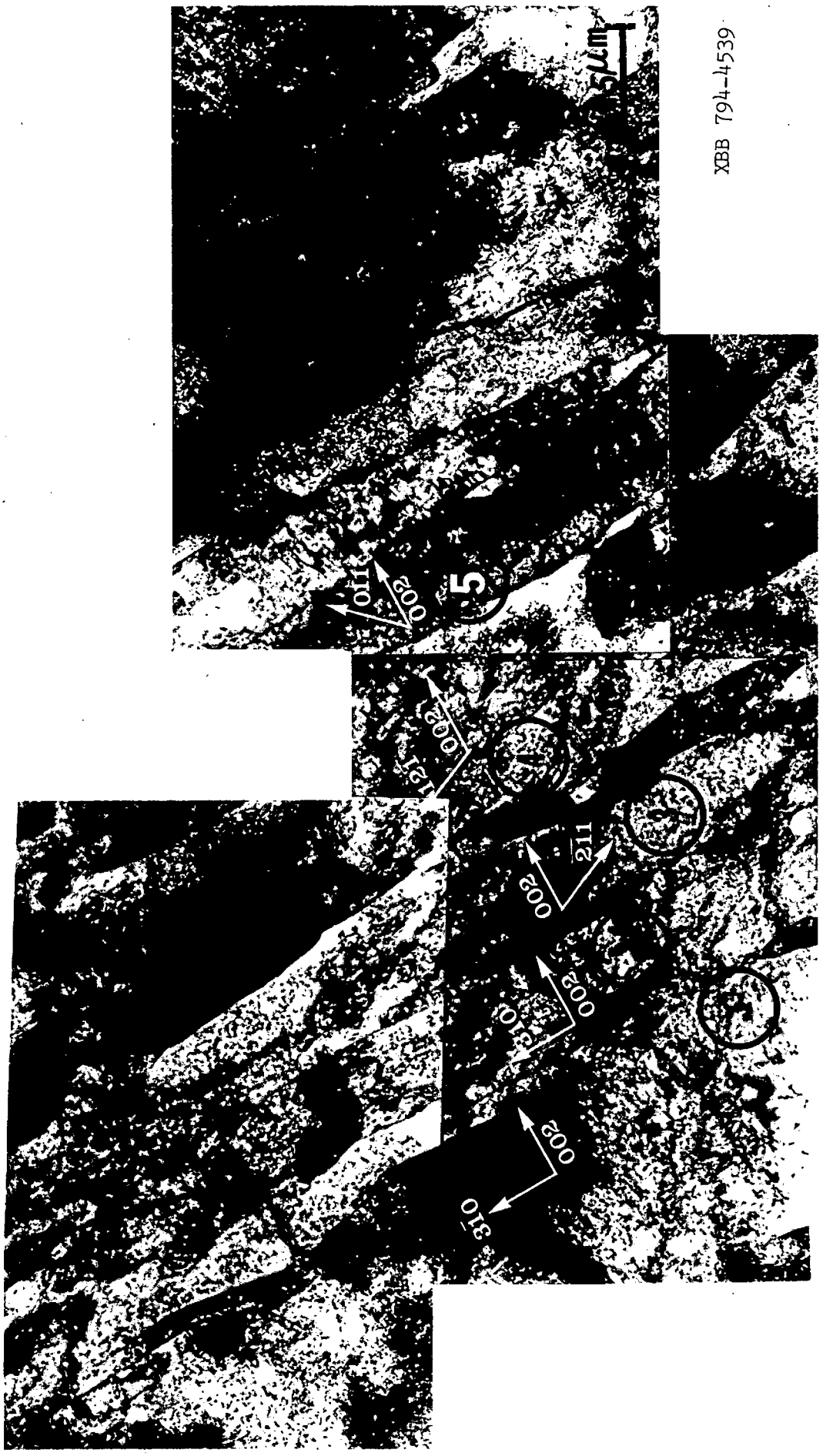

XBB 794-4539

Fig. 1a

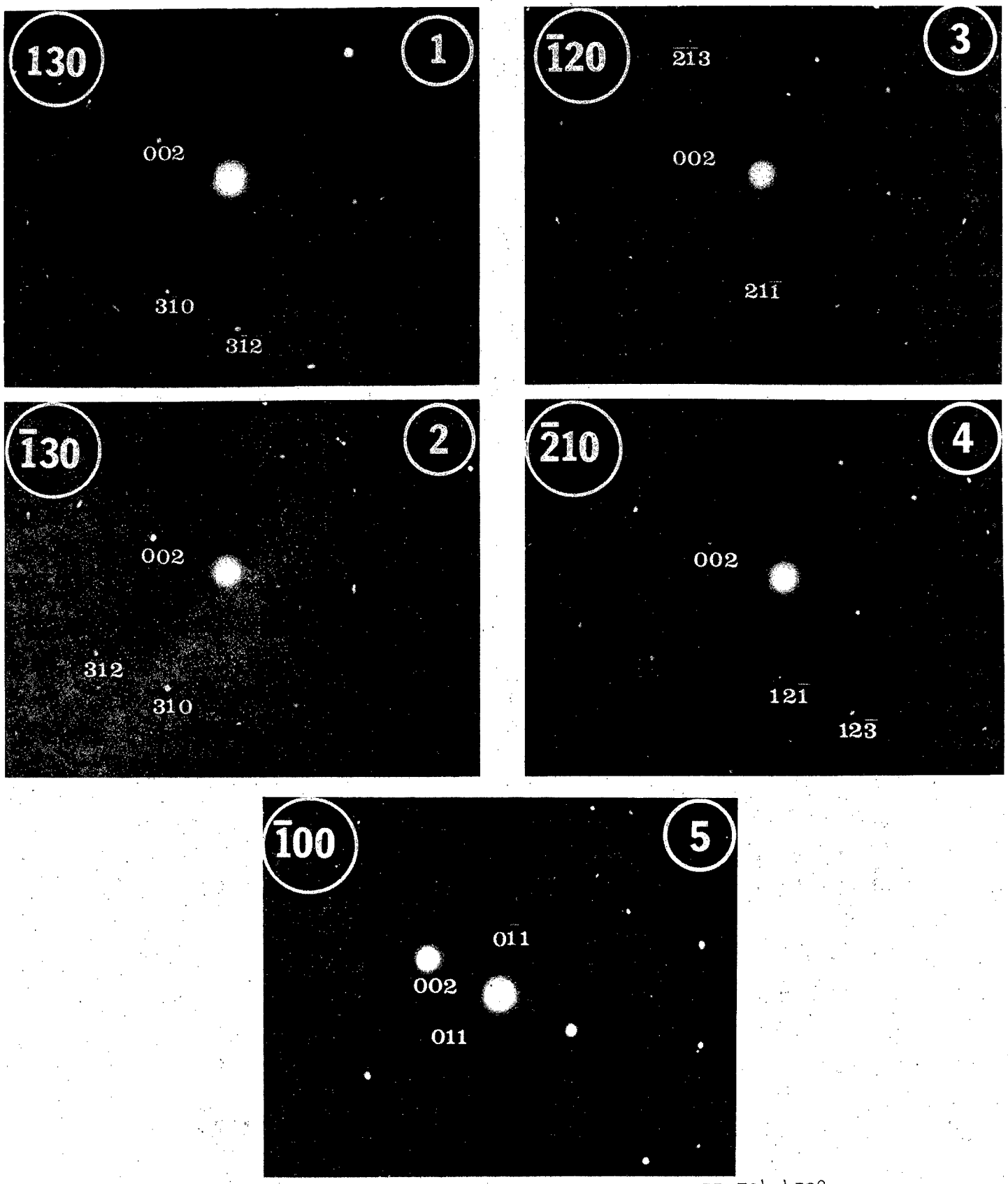

XBB 794-4538

Fig. 1b

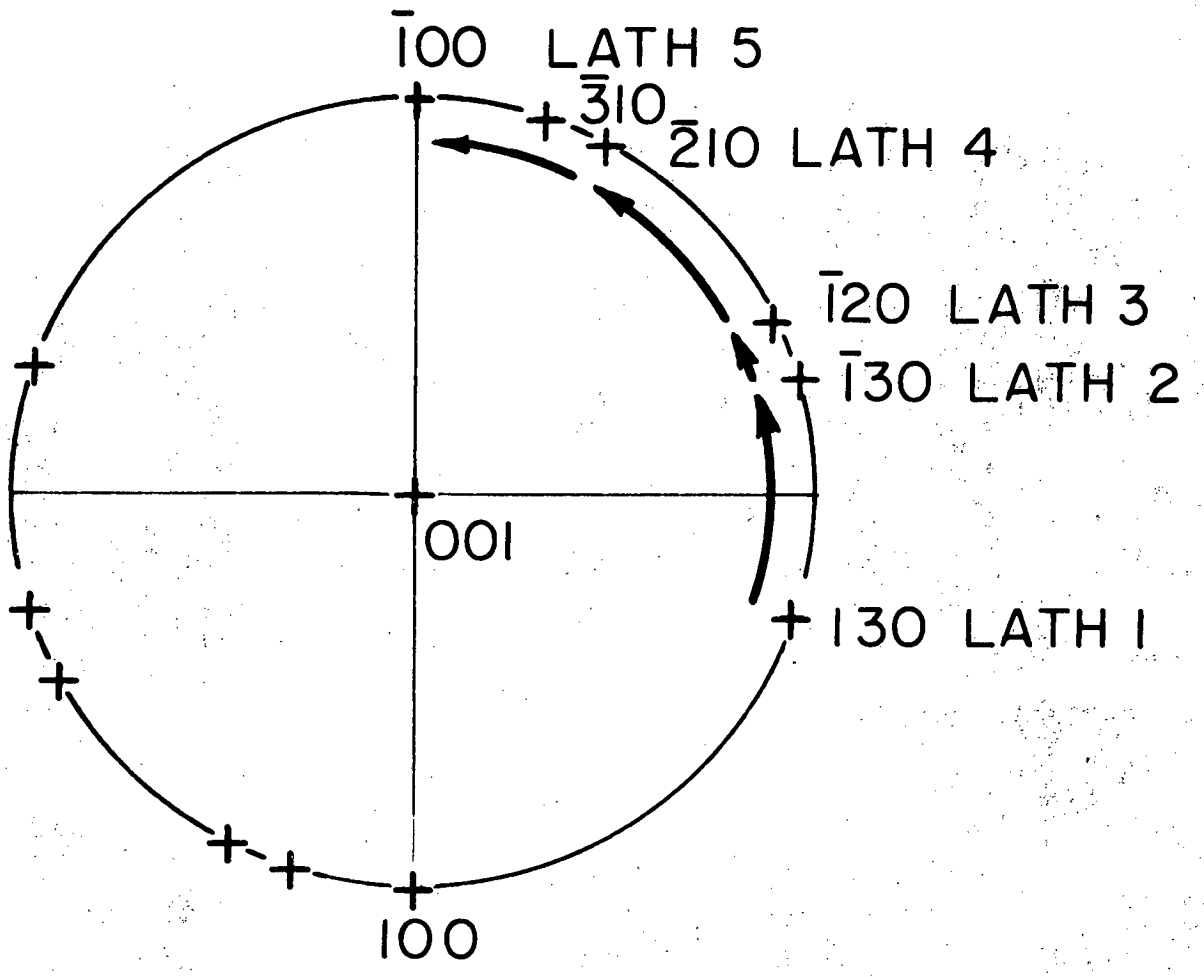

Lath Region		Rotation
From	To	(degrees)
1	2	36.86
2	3	8.13
3	4	36.88
4	5	26.56
		108.43 TOTAL

XBL 794-6071

Fig. 1c

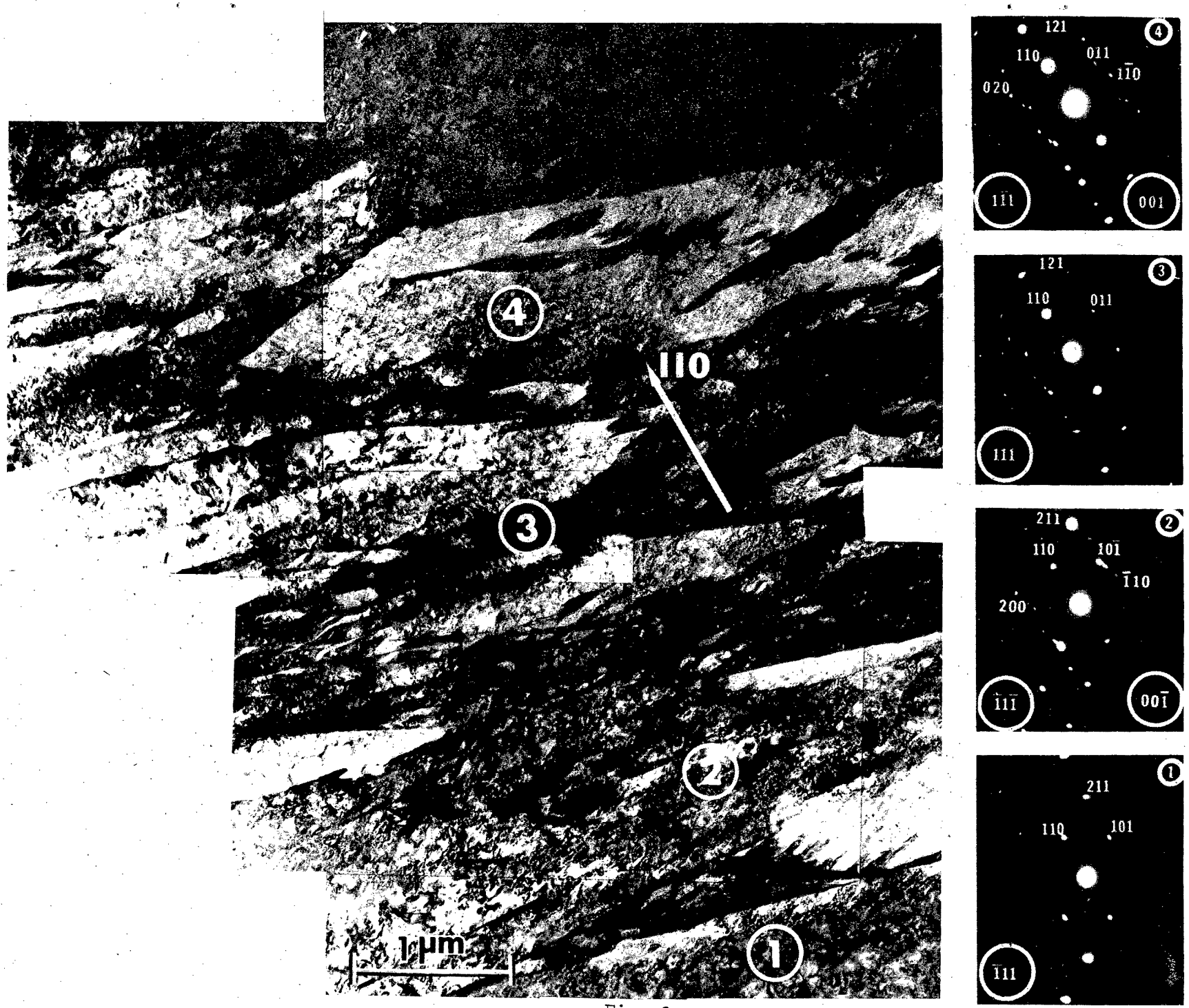
4
110
3
2
1
1μm
121
110
011
1̄10
020
1̄11
001
121
110
011
111
211
110
101
1̄10
200
1̄11
00ī
211
110
101
1̄11

Fig. 2a

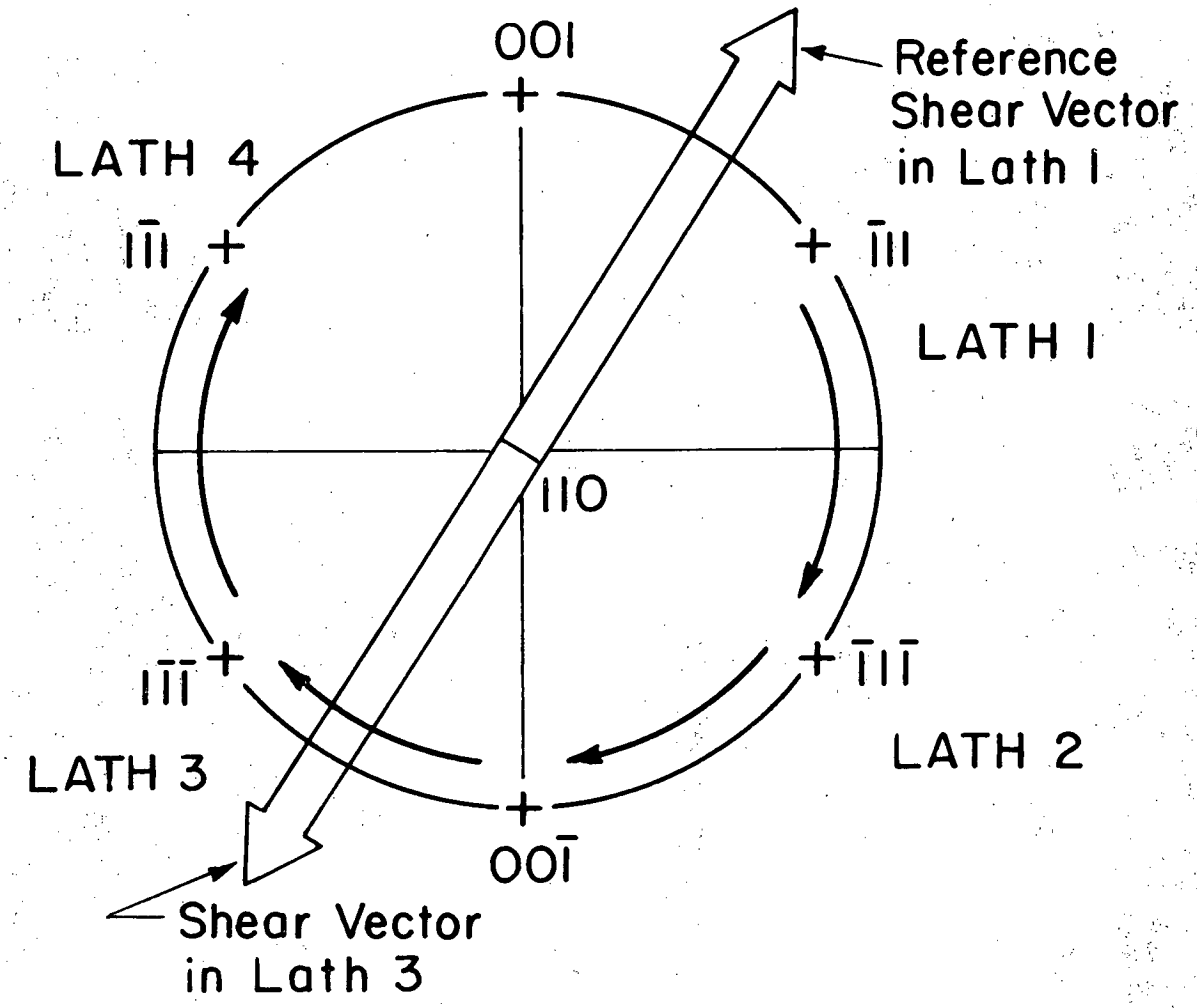

Lath Region		Rotation (degrees)
From	To	
1	2	70.53
2	3	109.47
3	4	70.53
		250.53 TOTAL

XBL 794-6073

Fig. 2b

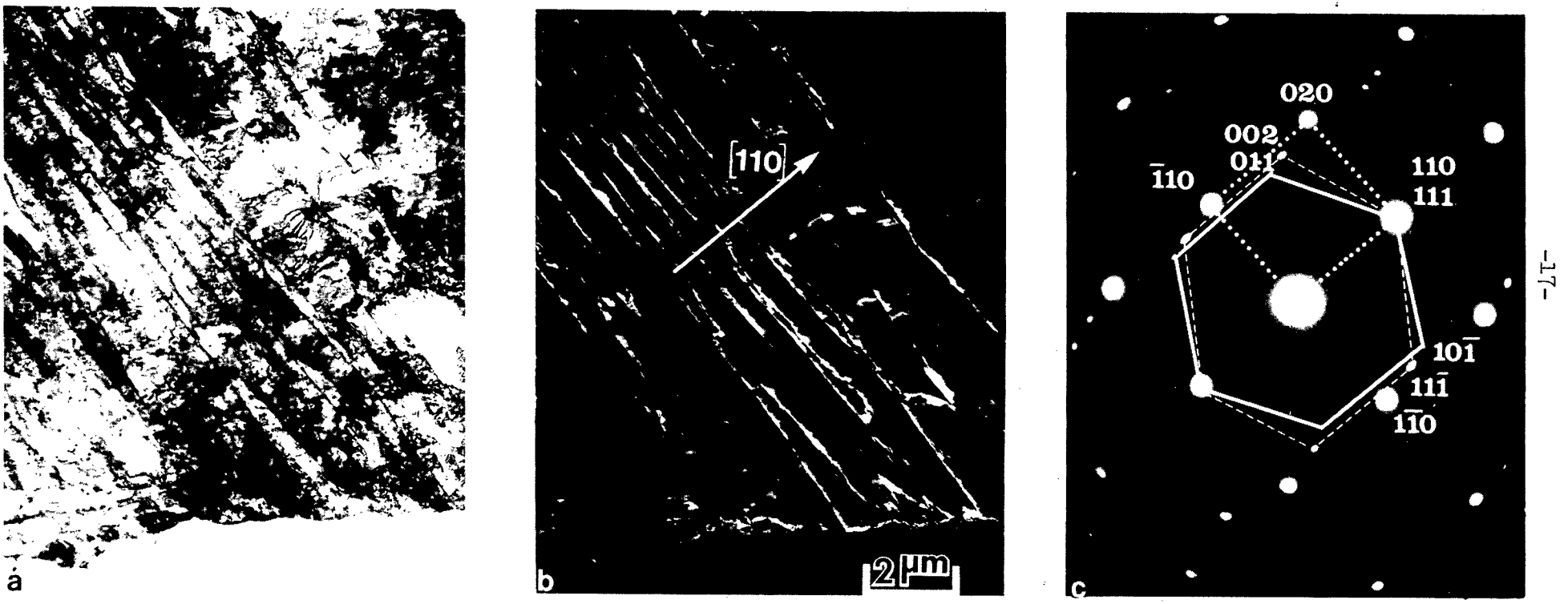

XBB 794-4537

Fig. 3

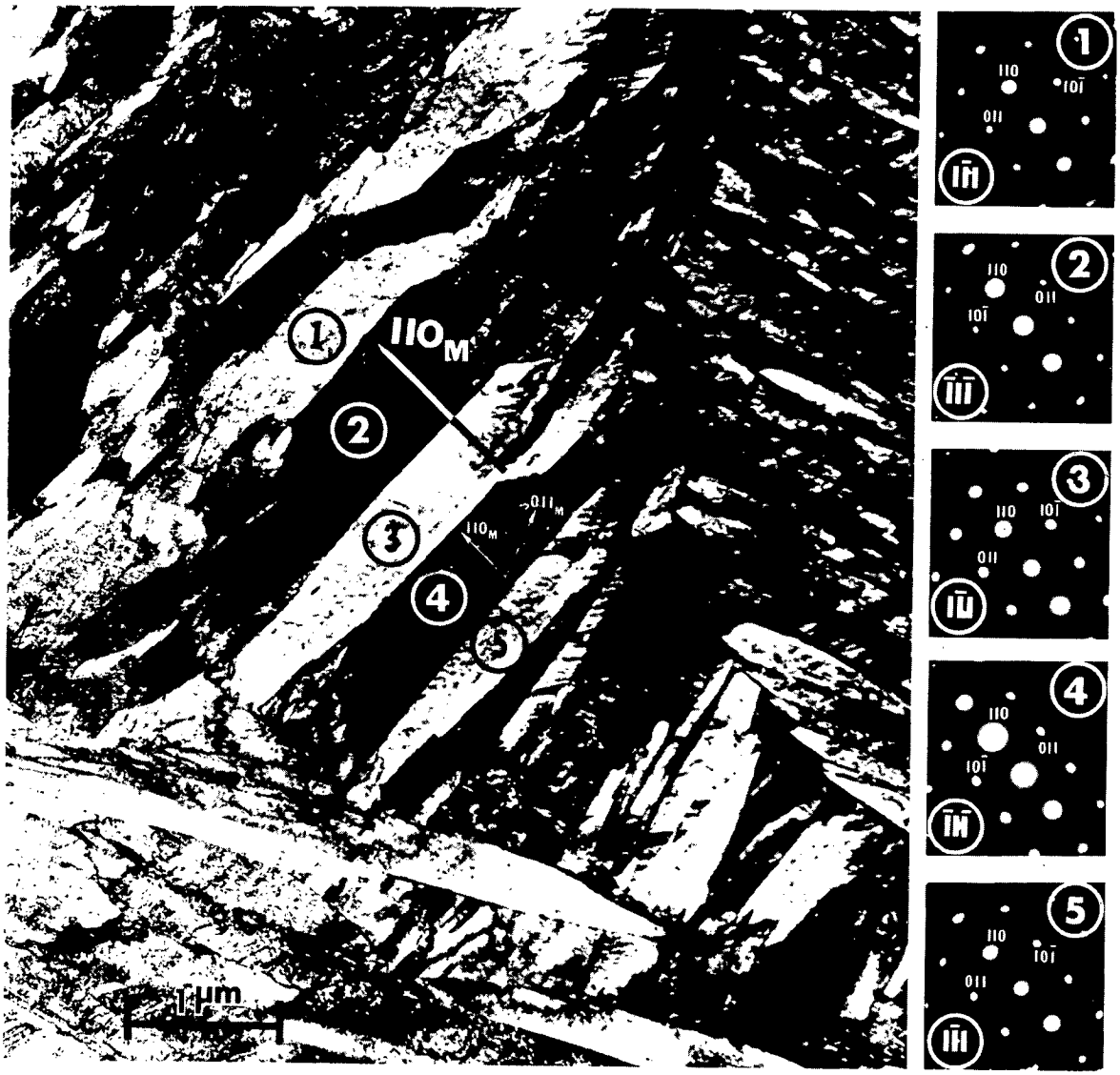

XBB 796-4250

Fig. 4

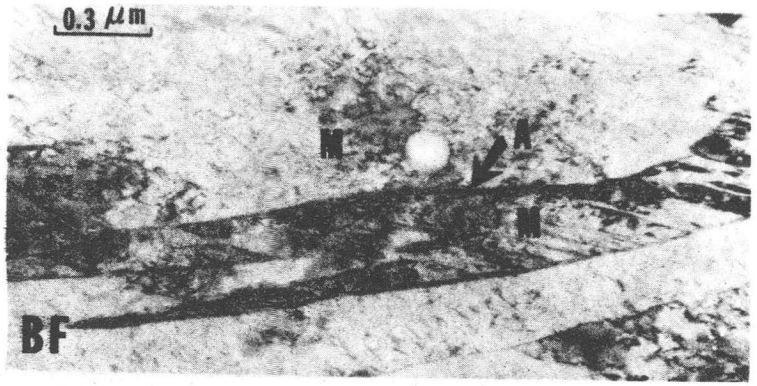

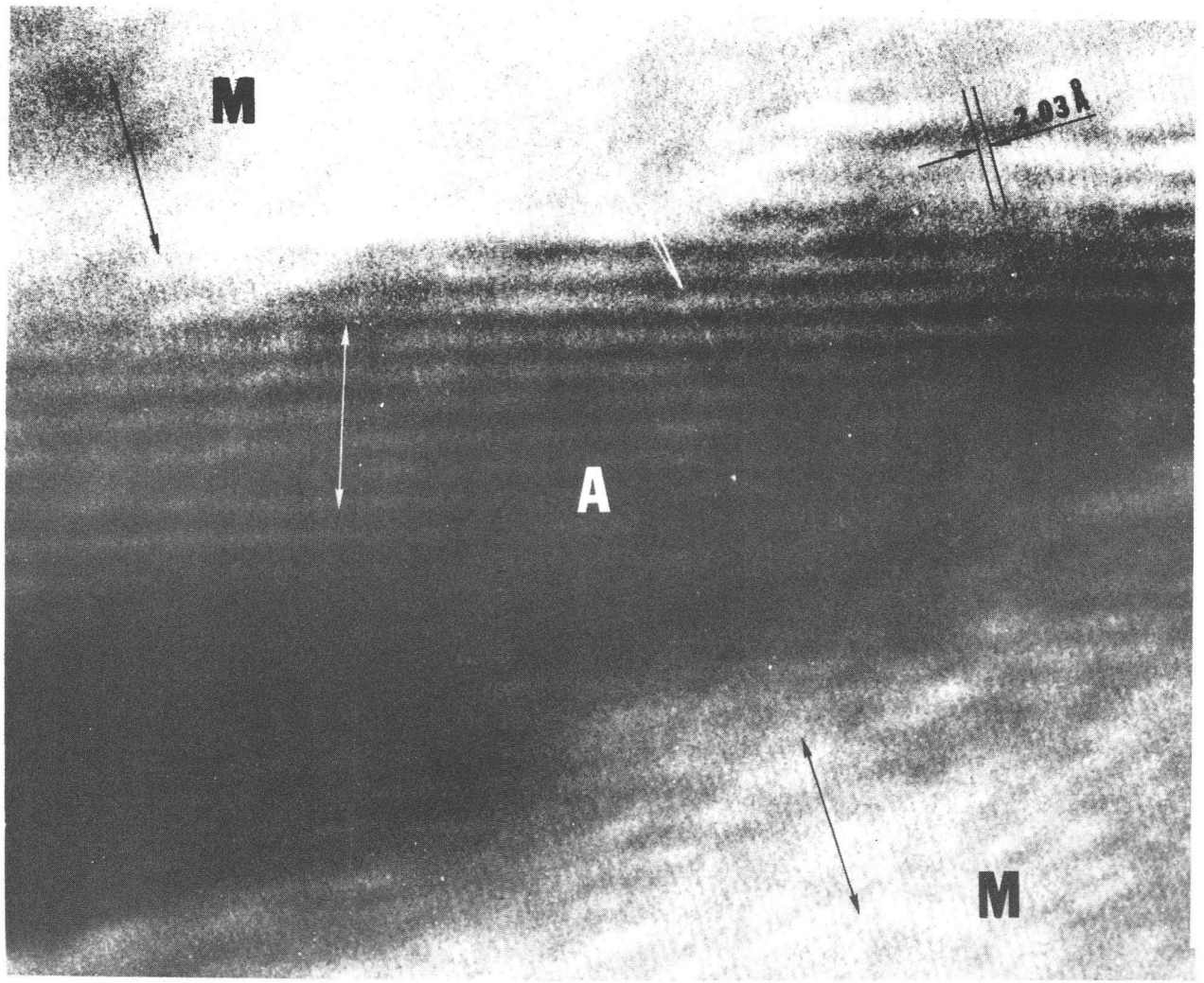

Fig. 5

XBB 782-2081

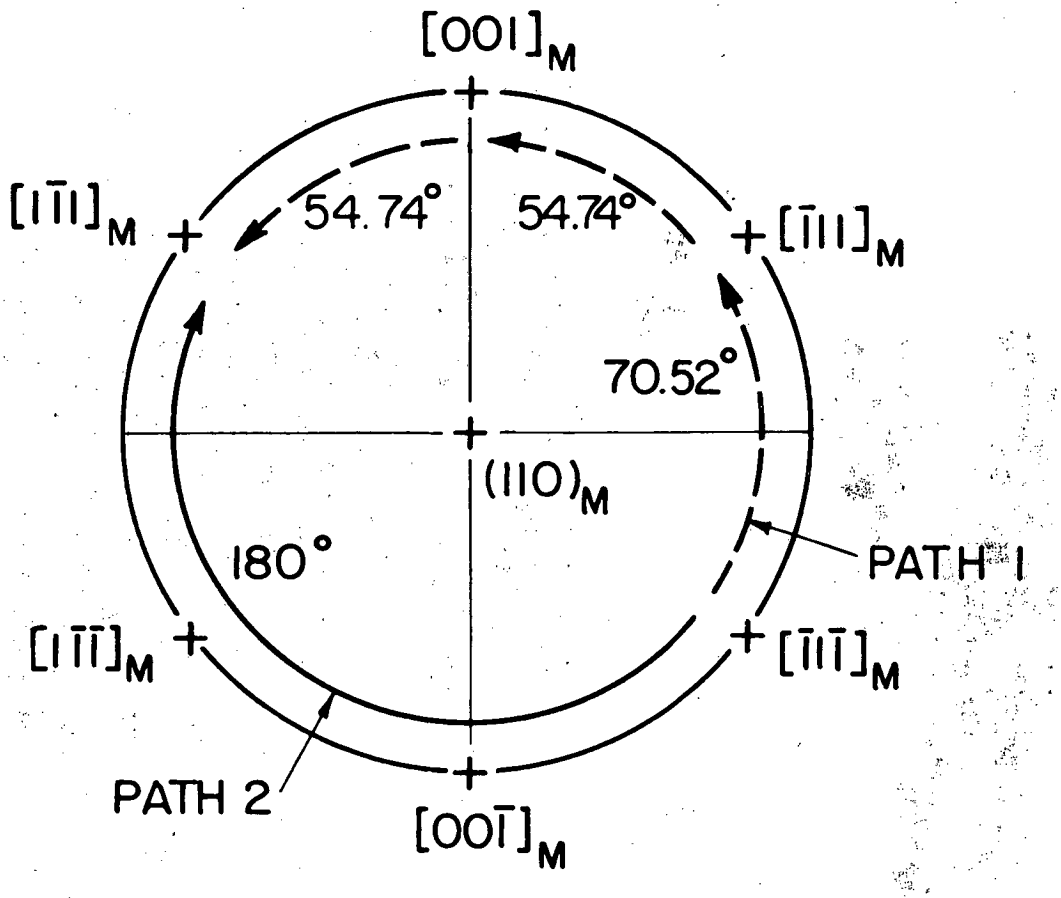

XBL794-6072

Fig. 6

TECHNICAL INFORMATION DEPARTMENT
LAWRENCE BERKELEY LABORATORY
UNIVERSITY OF CALIFORNIA
BERKELEY, CALIFORNIA 94720